Regular article

A peak position comparison method for high-speed quantitative Laue microdiffraction data processing

Jiawei Kou [a], Kai Chen [a,*], Nobumichi Tamura [b]

[a] Center for Advancing Materials Performance from the Nanoscale (CAMP-Nano), State Key Laboratory for Mechanical Behavior of Materials, Xi'an Jiaotong University, Xi'an, Shaanxi 710049, PR China
[b] Advanced Light Source, Lawrence Berkeley National Laboratory, Berkeley, CA 94720, USA

ABSTRACT

Indexing Laue patterns of a synchrotron microdiffraction scan can take as much as ten times longer than collecting the data, impeding efficient structural analysis using this technique. Here a novel strategy is developed. By comparing the peak positions of adjacent Laue patterns and checking the intensity sequence, grain and phase boundaries are identified, requiring only a limited number of indexing steps for each individual grain. Using this protocol, the Laue patterns can be indexed on the fly as they are taken. The validation of this method is demonstrated by analyzing the microstructure of a laser 3D printed multi-phase/multi-grain Ni-based superalloy.

© 2017 Acta Materialia Inc. Published by Elsevier Ltd. All rights reserved.

Although achieved earlier [1], polychromatic X-ray Laue diffraction was quickly superseded by monochromatic X-ray diffraction for structure analysis, because of the difficulties in interpreting the intensities. With the advent of synchrotron sources and the development of X-ray focusing optics, new applications for Laue diffraction have become possible, utilizing micro- or even nano-sized intense polychromatic X-ray beams under the form of Laue microdiffraction (μXRD) [2]. By scanning the crystalline sample surface with the focused X-ray probe and taking a Laue pattern (LP) at each position using a two-dimensional (2D) detector, this technique has been successfully applied to a range of scientific problems, including phase identification of tiny crystals [3], phase transformation at multi-scales [4,5], crystal orientation mapping [6], elastic strain/stress measurement [7,8], and defect quantification [9–11]. Since the spatial resolution is determined by the X-ray probe size and scanning step, each experiment usually collects massive number of LPs. Due to the high flux of synchrotron X-ray beam, only single exposure of 1 s or less is necessary to record a LP on a bulk crystal. However, analyzing a LP is not trivial. First, the Laue diffraction peak positions are determined accurately after removing background signal from the LPs. Second, for indexing the Laue peak positions are fitted with calculated ones based on a given crystal structure to derive crystal orientation and Miller indices of each diffraction peak. The indexing process may need to be repeated several times, depending on how many possible phases exist in the X-ray scanned area. Finally, refinement is performed to measure the lattice strain by taking into account the tiny deviations between the experimental Laue peak positions and the theoretical ones. This three-step analysis protocol is repeated sequentially and independently for all the LPs of a scan to map the phase, orientation, and strain distribution, which, for most polycrystalline samples, takes time on a regular desktop computer, much longer than that needed for data collection. This makes it incompatible with the study of complex materials with multiple phases, non-uniform grain size, or inhomogeneous defect distribution. For these materials researchers sometimes want to first scan a large area with coarse step size, and then after analyzing the data, map the microstructure of one or more selected areas of interests with finer steps. In these cases, faster data analysis is required. A close look at the conventional data analysis protocol reveals that over 70% of the time is consumed on the indexing process for single phase analysis by using the custom developed X-ray Microdiffraction Analysis Software (XMAS) [12], and up to 95% for multiple phases, indicating that indexing is the bottleneck of the analysis. Therefore, it is essential to shorten the time required to index the Laue scans, each of which contains thousands of LPs or even more.

In this study, we developed a new strategy to reduce the number of LPs that need to be indexed. Using the so-called peak position comparison (PPC) method, high-angle grain boundaries (HAGBs) and phase boundaries (PBs) are mapped rapidly. Only one LP needs to be indexed for each grain to assign the Miller indices to each reflection on the pattern, while the accurate orientation and lattice

---

* Corresponding author.
 E-mail address: kchenlbl@gmail.com (K. Chen).

strain distribution can be obtained by carrying out a pattern-by-pattern refinement, which takes much shorter time than indexing. This strategy is employed to study the microstructure of both the epitaxial and stray grain region in a laser 3D printed Ni-based superalloy. A cross-check between the results obtained using the PPC method and the output from XMAS proves the analysis accuracy and reliability. More importantly, by applying the PPC strategy, simultaneous data analysis becomes realistic even on a regular personal computer as the μXRD scan is performed, raising the possibility of real-time analysis to facilities that do not have easy access to supercomputers.

The appearance of PBs and HAGBs is evidenced by a significant change of peak positions between two adjacent LPs. Here 'significant' is emphasized because a slight peak shift are more likely induced by local lattice strain or defects, in which case the indexing result from the previous LP is still valid. Consequently, it is necessary to quantify the peak position change on the 2D detector as a function of disorientations. For convenient description, a detector coordinate system **O-xy** is established, in which the original position **O** is fixed at the bottom left corner of the detector, **x**- and **y**-axes are parallel with the horizontal and vertical edges of the detector, respectively, and the unit length equals to the detector pixel size d_p. Any point P (x, y) on the detector can be expressed by vector **k** that points from the X-ray focal point to P:

$$\mathbf{k} = \mathbb{A} \cdot \begin{bmatrix} (x-x_c) \cdot d_p \\ (y-y_c) \cdot d_p \\ 0 \end{bmatrix} + \begin{bmatrix} 0 \\ 0 \\ d \end{bmatrix} \tag{1}$$

where (x_c, y_c) is the coordinate of the projection position of the X-ray focal point on the detector, and d is the focal point to detector distance. **A** is a transformation matrix defined by the tilt of the detector:

$$\mathbf{A} = \begin{pmatrix} \cos\theta \cdot \cos\phi & \cos\phi \cdot \sin\theta & -\sin\phi \\ \cos\theta \cdot \sin\psi \cdot \sin\phi - \cos\psi \cdot \sin\theta & \cos\psi \cdot \cos\theta + \sin\psi \cdot \sin\theta \cdot \sin\phi & \cos\phi \cdot \sin\psi \\ \cos\psi \cdot \cos\theta \cdot \sin\phi + \sin\psi \cdot \sin\theta & \cos\psi \cdot \sin\theta \cdot \sin\phi - \cos\theta \cdot \sin\psi & \cos\psi \cdot \cos\phi \end{pmatrix}^{-1} \tag{2}$$

where θ, ψ, and ϕ denote the yaw, pitch, and roll of the detector (as shown in Fig. S1 in the Supplementary material), respectively, and usually ϕ is set to be 0. By combining Eqs. (1) and (2), the angle between any two positions on the detector can be calculated.

To employ the PPC methods, only the very first LP needs to be analysed following the conventional approach. An example of such indexed pattern is shown in Fig. 1a, with the Miller indices marked for each reflection. In a second step, a threshold deviation angle δ is defined by the user, depending on the deformation status. Usually higher threshold angle δ is assigned to highly deformed samples. In this example, δ is set to be 2°. The detector area within 2° around each peak is calculated and marked with dashed ellipses in Fig. 1. Then the Laue peaks in the adjacent patterns will be checked. If most of the peaks fall inside the ellipses, as shown in Fig. 1b, the Miller indices will be assigned to each peak in the new pattern, without calling the indexing algorithm. In the example, comparing the two patterns in Fig. 1a and b, three peaks are missing, resulting from the low signal to noise ratio of the intrinsically weak $0\bar{2}8$ and $\bar{3}\bar{1}9$ reflections, and/or the existence of blind areas on the detector such as for the $\bar{1}\bar{1}9$ reflection. In our computer program, user input parameters are therefore available to define a tolerance as a percentage of missing reflections. In this example, it is defined that if a reflection is found in 70% of the ellipses, these two patterns are regarded to be recorded from a same crystal grain. If most of the peaks, however, fail to fall inside the ellipses, as displayed in Fig. 1c, the indexing algorithm has to be called to obtain the Miller indices of all the peaks. Sometimes a couple of peaks may still fall into the ellipses even if the orientation changes, such as for the $\bar{2}06$ reflection in Fig. 1c, which is also taken into account in our program. In either case, once the Miller indices of each reflection is known, a rapid interior point algorithm [13] based orientation refinement is carried out to get the accurate crystal orientation, by minimizing the sum of the deviation angles between each experimental peak position and the calculated ones [12]. Afterwards a Nelder-Mead Simplex algorithm [14] based strain refinement is employed, similar to the one used in XMAS, to map the deviatoric strain distribution quantitatively. With this strategy, in theory, each crystal grain needs to be indexed only once, while for all other scanning points only refinements are necessary. Although in real case, more than one pattern needs to be indexed due to the significant Laue peak position change induced by high density of intragranular defects, the total analysis time can be still greatly cut down, no matter only single phase is considered, or multiple phases need to be indexed.

Because of the large penetration depth of the high energy synchrotron X-ray beam, diffraction may take place on more than one crystal grain and each grain will generate a set of Laue peaks (Fig. S2). Using the differential aperture method [15], the orientation distribution along the depth direction can be mapped, while aperture scan experiment and analysis take extremely long time. More conventionally, the strongest set of Laue peaks will be selected as the dominant signal at the scanning position, and its corresponding structure and orientation
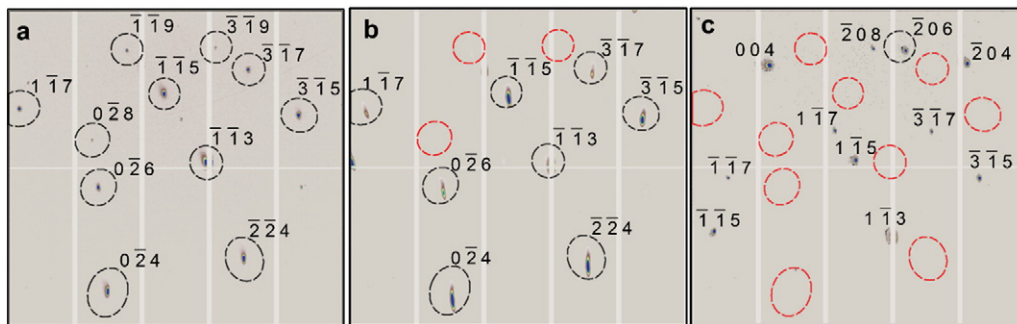
Fig. 1. A schematic explanation of the PPC method. (a) An indexed pattern with all Miller indices marked and the ellipses round each peak shows a tolerance region of 2°. (b) A Laue pattern taken in the same grain as (a), with all peaks falling in the ellipses except several missing ones. (c) A Laue pattern taken in a different grain.

are plotted in the 2D microstructure map. To adapt this custom, the intensities of the reflections falling in the ellipses are compared to all other peaks that show up in the same LP but not in the ellipses. If most of them are among the strongest ones, the indexing process will be skipped; otherwise the LP needs to be indexed. Alternatively, if the μXRD scan step is fine enough (less than the X-ray beam size, for example), the intensity of the reflections with the same Miller indices from the same crystal grain will keep approximately constant or vary proportionally, until meeting a grain or phase boundary.

To verify the data analysis strategy, a laser 3D-printed Ni-based superalloy with enriched microstructure features was studied using the μXRD technique. The specimen substrate was cut from a {100} directionally solidified DZ125L superalloy ingot. Powders of similar element composition with the diameters of 50 to 100 μm were coaxially injected and melted into the molten pool formed by a laser beam. By optimizing the processing parameters, cladding materials epitaxial to the substrate were obtained [16,17], although eventually the epitaxy was lost and equiaxed stray grains were formed due to the defect accumulation induced dynamical recrystallization or inhomogeneous nucleation [18]. Two areas on the mirror-finish polished cross-section of the 3D printed sample, mounted on a high resolution scanning stage tilted 45° relative to the incident X-ray beam, were scanned with the micro-focused polychromatic (5–24 keV) X-ray probe on Beamline 12.3.2 at the Advanced Light Source of the Lawrence Berkeley National Lab [19]. The substrate-cladding interface was aligned with the horizontal scan direction. The scanned regions consist of a 250 μm (horizontal) × 352 μm (vertical) area close to the substrate-cladding interface with scanning step sizes of 2 μm and 4 μm in horizontal and vertical directions, respectively, and of a 80 μm × 80 μm area with 2 μm step size in the stray grain region. At each scanning position, a LP was recorded in reflection mode with a 2D DECTRIS Pilatus-1 M detector, mounted about 150 mm above the X-ray focal point and 90° with respect to the incident X-ray. To further investigate the applicability, a μXRD scan taken on a thin-sectioned naturally deformed quartz specimen was analysed using the PPC method and summarized in the Supplementary material (Figs. S2 and S3).

The LPs taken from the stray grain region were first analysed, considering the face-centered cubic (FCC) Ni phase only, using the PPC method with and without checking the reflection intensity, respectively, to map the grain boundary distribution, as shown by the thick red curves in Fig. 2a and b. Since the grain sizes in the scanned region was tens of microns, which was comparable with the X-ray penetration depth, a considerable fraction of the grain boundaries were missing when the reflection intensity was not checked. It was found that for FCC metals, if more than four of the eight strongest peaks fell inside the ellipses, the LP could be regarded as being taken in the same grain. Such intensity check criterion secured a more reasonable 2D grain boundary distribution map, which was almost identical with the output from XMAS, displayed as the thin black curves in the same map. Consequently, it is concluded that the intensity check practice is necessary and effective, especially for the polycrystalline or multi-phase materials where the crystal grains are not significantly bigger than the X-ray penetration depth. The advantage of the PPC method is obvious regarding time consumption. To obtain the grain boundary distribution map in Fig. 2b, background removal is not necessary and the reflection peak positions do not need to be accurate, so the analysis took less than 15 min on a personal computer, much shorter than the data collection time (~50 min). To map the orientation and strain distribution, the indexing routine was triggered only 35 times, among all the 1600 LPs. Thus the analysis was completed within 45 min, comparable to the data collection time. It is also noticed that with different intensity check criterion, the grain morphologies and HAGB positions will vary. With a more critical criterion, the HAGB position is more like to coincide with the results output by using XMAS, but then more indexing routines will be triggered and thus longer analysis will be required.

It had been known that the carbide precipitates in the cladding layers were at the nanoscale, which did not generate strong Laue diffraction signals under the experimental condition [20]. Thus only the FCC Ni phase was considered for the stray grain region data analysis. Since the carbides were several microns in size in the substrate, thus the LP taken at each scanning position was fitted with both the FCC and MC (M = Ti, W, Ta, Nb) carbide phase to map the phase and orientation distributions simultaneously. Since both phases belong to the $0Fm\bar{3}m$ space group while the lattice constant of MC is about 25% larger than Ni, these two phases were identified by a comprehensive consideration of the numbers of indexed and missing reflections. Missing reflections are those with non-zero structure factor but undetectable intensity. To apply the PPC method, the intensity check parameters are set as 'three of the five strongest peaks in ellipses' and 'five of the twelve strongest peaks in ellipses' for Ni and MC phases, respectively. The phase distribution is displayed in Fig. S6. The orientation distribution map was demonstrated in Fig. 3a. From the peak width and disorientation distribution maps, the scanned region could be divided into three regions, which were the unaffected substrate at the bottom (3375 LPs), heat-affected zone (HAZ) in the middle (4250 LPs), and the cladding layers on top (3375 LPs). Micro-sized particles in the substrate and HAZ were MC carbide precipitates, while all other areas
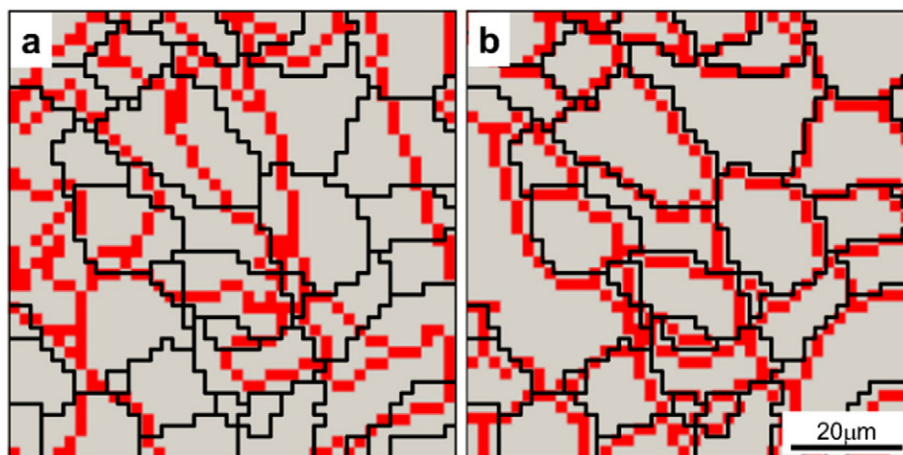

Fig. 2. Grain boundary map of the stray grain area (a) without and (b) with intensity check. Black and red curves show the HAGBs detected using the conventional and the PPC methods, respectively.
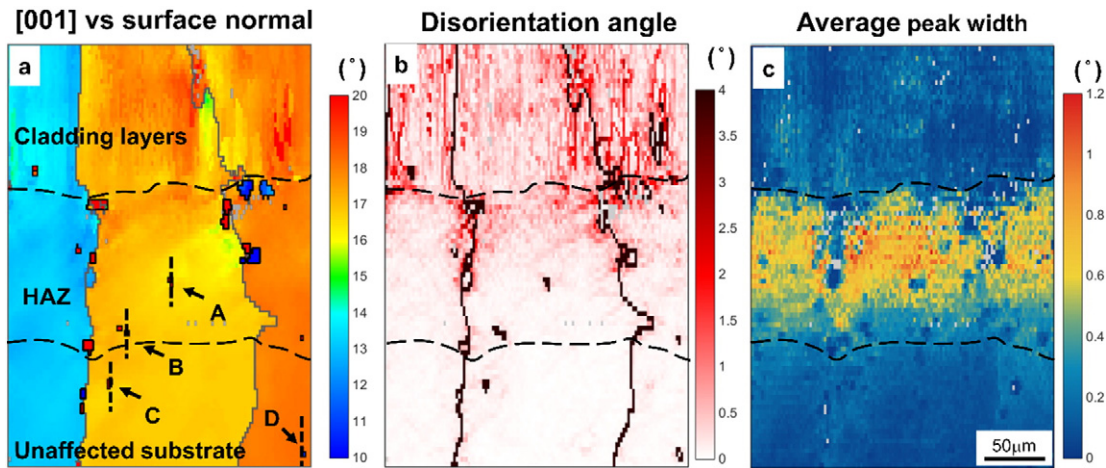
Fig. 3. Maps of (a) crystal orientation, (b) disorientation angle, and (c) average peak width distribution.

were indexed as FCC metal phase. Three columnar grains were detected, with the HAGBs roughly perpendicular to the substrate/cladding interface. No straightforward orientation relationship between the metallic phase and the MC were derived. The crystal orientation of each grain in the substrate was uniform, thus in this region the indexing process was scarcely called resulting in very fast analysis. A slightly larger fraction of LPs needed to be indexed independently for the plastically deformed HAZ because the orientation became non-uniform and the Laue peaks were broadened, resulting from the thermomechanical impacts of the laser heating and the steep temperature gradient from the melting pool to the substrate. It was found that about 5.9% of LPs in HAZ failed to be indexed using the conventional method, while with PPC method, the orientation was not successfully mapped in only about 0.08% of the scanning positions. Such increased indexing capability was attributed to the following fact. In HAZ the Laue peaks were broadened and the peak intensity was low, thus peak searching was not as effective resulting in failed indexation. With the PPC method, on the other hand, indexing was infrequently necessary, thus the orientation could still be obtained no matter how successful the peaks were searched. The orientation was even more inhomogeneous in the cladding layers, where the Laue reflections became split due to the rapid solidification induced high density of defects. If several subpeaks appeared in the calculated ellipses, crystal orientation could not be obtained via refinement only and thus the indexing process was triggered more frequently. As summarized in Table 1, only ~800 LPs were indexed for the whole scan of 11,000 LPs to map distributions of the MC carbide precipitates and the orientation of each phase and each crystal grain. The analysis took only 6.4 h, just 15 min longer than data collection. Although it should be admitted that the analysis will take longer time if more phases, finer grains, and more badly deformed crystals are involved, PPC method can speed up the data analysis dramatically and provide a promising approach toward real time microstructure mapping based on the μXRD scans.

Although finer scans were not made in this sample due to the limited synchrotron beam time accessible to us, we note that detailed microstructure study could be carried out based on the orientation/phase distribution map. The plastic deformation around the MC carbide particles was characterized from the full width at half maximum (FWHM) of a selected Laue peak appearing close to the center of the 2D detector. For example, the FWHM along the vertical dashed lines across the MC particles marked from A to D were studied and plotted in Fig. 4, with the horizontal axis showing the distance from the scanning position to the HAZ-cladding layer interface. There is an overall trend that the farther from the interface, the sharper the peaks are. Moreover, the peak width increased significantly across each MC particle, offering direct evidence to local defect accumulation and stress concentration owing to the mismatch of the coefficients of thermal expansion and moduli between the metallic phase and the carbides. It is believed that the mismatch is harmful for the mechanical properties of Ni-based superalloy, and may be responsible for the formation of microcracks during welding process [21,22].

In summary, a novel method has been developed to dramatically accelerate the analysis of Laue μXRD scan datasets. Within each crystal grain, the phase and orientation can be obtained without indexing the LPs, by comparing the peak positions of adjacent scanning positions. Independent indexing process is necessary only at the HAGBs, PBs, or when several subgrains are observed in one single LP. With this strategy, the microstructure can be mapped rapidly. Two examples from laser 3D printed Ni-based superalloy demonstrated the usefulness of our approach. The grain boundary mapping of the stray grains shows that intensity check is important and effective for polycrystal study. For a dual phase area at the substrate-cladding interface, phase, orientation, disorientation angles, and average peak width distributions are plotted almost in sync with data collection in real time, on a common personal computer, and more detailed microstructure study is carried out based on the phase/orientation map.

Table 1

Analysis of the μXRD scan data of the substrate-cladding interface area of a laser 3D printed Ni-based superalloy.

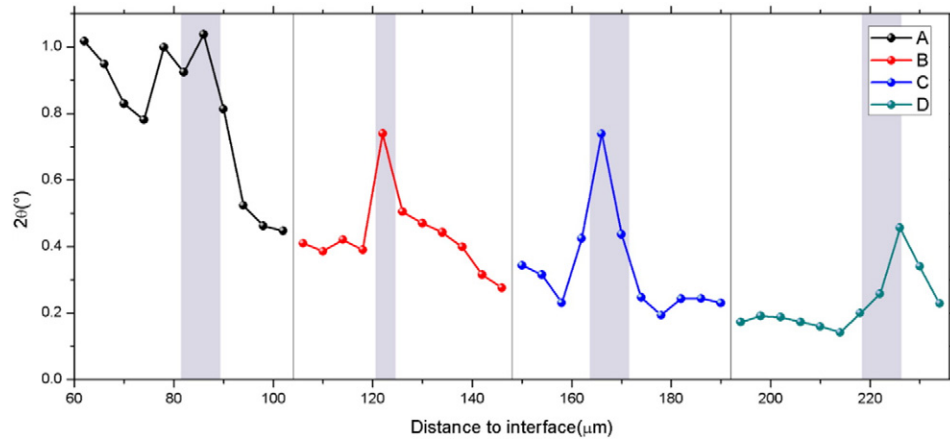| Zone	Index called	Pattern no.	Percentage of indexing
Cladding	441	3375	13.7%
HAZ	333	4250	7.84%
Substrate	32	3375	0.95%
Sum	806	11,000	7.33%

Fig. 4. Average peak width along the dashed lines shown in Fig. 3 across multiple MC precipitates.

Acknowledgements

Appendix A. Supplementary data

Supplementary data to this article can be found online at http://dx.doi.org/10.1016/j.scriptamat.2017.09.005.

References

[1] W. Friedrich, P. Knipping, M. Laue, Acad. Wiss. Munich 42 (1912) 303.
[2] G.E. Ice, B.C. Larson, W. Yang, J.D. Budai, J.Z. Tischler, J. Pang, R. Barabash, W. Liu, J. Synchrotron Radiat. 12 (2005) 155.
[3] C. Dejoie, P. Sciau, W. Li, L. Noe, A. Mehta, K. Chen, H. Luo, M. Kunz, N. Tamura, Z. Liu, Sci Rep 4 (2014) 4941.
[4] H. Guo, K. Chen, Y. Oh, K. Wang, C. Dejoie, S.A. Syed Asif, O.L. Warren, Z.W. Shan, J. Wu, A.M. Minor, Nano Lett. 11 (2011) 3207.
[5] B.S. Mun, K. Chen, J. Yoon, C. Dejoie, N. Tamura, M. Kunz, Z. Liu, M.E. Grass, S.-K. Mo, C. Park, Y.Y. Lee, H. Ju, Phys. Rev. B 84 (2011) 113109.
[6] E.Y. Ma, Y.-T. Cui, K. Ueda, S. Tang, K. Chen, N. Tamura, P.M. Wu, J. Fujioka, Y. Tokura, Z.-X. Shen, Science 350 (2015) 538.
[7] K. Chen, M. Kunz, N. Tamura, H.R. Wenk, Geology 43 (3) (2015) 219–222.
[8] M. Kunz, K. Chen, N. Tamura, H.-R. Wenk, Am. Mineral. 94 (2009) 1059.
[9] T. Ohashi, R.I. Barabash, J.W.L. Pang, G.E. Ice, O.M. Barabash, Int. J. Plast. 25 (2009) 920.
[10] D. Qian, A. Zhang, J. Zhu, Y. Li, W. Zhu, B. Qi, N. Tamura, D. Li, Z. Song, K. Chen, Appl. Phys. Lett. 109 (2016) 101907.
[11] A. Lupinacci, K. Chen, Y. Li, M. Kunz, Z. Jiao, G.S. Was, M.D. Abad, A.M. Minor, P. Hosemann, J. Nucl. Mater. 458 (2015) 70.
[12] N. Tamura, in: R. Barabash, G. Ice (Eds.), Strain and Dislocation Gradients From Diffraction: Spatially-resolved Local Structure and Defects, Imperial College Press, London 2014, pp. 125–155.
[13] R.A. Waltz, J.L. Morales, J. Nocedal, D. Orban, Math. Program. 107 (2005) 391.
[14] J.C. Lagarias, J.A. Reeds, M.H. Wright, P.E. Wright, SIAM J. Optim. 9 (1998) 112.
[15] B. Larson, W. Yang, G. Ice, J. Budai, J. Tischler, Nature 415 (6874) (2002) 887–890.
[16] M. Gäumann, C. Bezençon, P. Canalis, W. Kurz, Acta Mater. 49 (2001) 1051.
[17] M. Gäumann, S. Henry, F. Cléton, J.D. Wagnière, W. Kurz, Mat. Sci. Eng., A 271 (1999) 232.
[18] Y. Li, D. Qian, J. Xue, J. Wan, A. Zhang, N. Tamura, Z. Song, K. Chen, Appl. Phys. Lett. 107 (2015) 181902.
[19] M. Kunz, N. Tamura, K. Chen, A.A. MacDowell, R.S. Celestre, M.M. Church, S. Fakra, E.E. Domning, J.M. Glossinger, D.W. Plate, B.V. Smith, T. Warwick, H.A. Padmore, E. Ustundag, Rev. Sci. Instrum. 80 (2009), 035108.
[20] G. Zhou, W. Zhu, H. Shen, Y. Li, A. Zhang, N. Tamura, K. Chen, Sci Rep 6 (2016) 28144.
[21] L.R. Liu, T. Jin, N.R. Zhao, X.F. Sun, H.R. Guan, Z.Q. Hu, Mat. Sci. Eng., A 361 (2003) 191.
[22] L.Z. He, Q. Zheng, X.F. Sun, H.R. Guan, Z.Q. Hu, A.K. Tieu, C. Lu, H.T. Zhu, Mat. Sci. Eng., A 397 (2005) 297.